Journal of Engineering Mathematics (2005) 53: 99–112
DOI 10.1007/s10665-005-9003-4

A multiphase model for the early stages of the hydration of retarded oilwell cement

J. BILLINGHAM, D.T.I. FRANCIS[1], †A.C. KING[1] and A.M. HARRISSON[2]
School of Mathematical Sciences, The University of Nottingham, University Park, Nottingham NG7 2RD, UK (E-mail: John.Billingham@nottingham.ac.uk) [1]*School of Mathematics and Statistics, The University of Birmingham, Edgbaston, Birmingham B15 2TT, UK;* [2]*The Rugby Group, RMC House, Rugby CV21 2DT, UK*

Received 17 November 2003; accepted in revised form 7 June 2005

Abstract. Cement is used in the oil industry to line oil wells. The major components of oilwell cement are tricalcium silicate (C_3S), dicalcium silicate (C_2S), tricalcium aluminate (C_3A) and calcium sulphate ($CaSO_4$). With the exception of C_2S, each of these plays an important role in the initial thickening of cement slurry. It is important to control the time that it takes for a slurry to thicken, and this is achieved by the addition of chemical retarders, which delay the onset of thickening. In this paper, the action of a retarder whose effects are firstly, to form a complex with calcium ions, and secondly, to inhibit the growth of ettringite crystals is investigated. Ettringite is a product of the hydration of C_3A and the subsequent reaction of the products with calcium sulphate. A modified version of a model for the hydration of C_3S previously investigated by Salhan, Billingham and King (*J. Engng. Math.* 45 (2003) 367), along with the chemical-kinetic scheme for the action of a retarder on ettringite proposed by Billingham and Coveney (*J. Chem. Soc. Faraday Trans.* 89 (1993) 3021) is used. The model distinguishes between liquid and solid phases, and treats water, which is significantly depleted by the formation of ettringite, as one of the chemical constituents. It is found that both of the chemical actions of the retarder contribute to slowing the initial reaction rate, and that the sudden crystallisation of ettringite as the effect of the retarder is overcome, investigated by Billingham and Coveney, occurs in successive layers around the surface of the cement grain.

Key words: cement hydration, numerical simulation, reaction-diffusion equations

1. Introduction

Oilwell cement is used to secure a cylindrical metal pipe in a newly drilled well, and thereby isolate the well from the surrounding formation. Accurate control of the thickening time, that is the time after initial mixing when the cement can no longer be pumped, is crucial in this process. If the thickening time is too short, the cement fails to reach its required placement, whilst too long a thickening time leads to costly delays, [1, Chapter 2]. It is usual to control the thickening time using chemical additives, known as retarders, typically phosphonates (see for example, [2]). The mechanism by which phosphonates and other chemicals act as retarders is not well understood, but it is known that retarders bind to calcium ions, [3, Chapter 11], and are able to inhibit the growth of ettringite crystals, [4, 5].

In an earlier paper, [6], we argued that the early stages of cement hydration are dominated by the hydration of the main constituent of oilwell cement, tricalcium silicate (C_3S), to form a calcium silicate hydrate gel (CSH) and calcium hydroxide (CH). Note that we are using the usual cement nomenclature where C represents calcium oxide, CaO, S represents silicate,

†Professor King died on 14 January 2005.

SiO_2, and H represents water, H_2O. We developed a model that agrees well with experimental results, in terms of the rate at which calcium ions are produced. We have also considered and quantified the effect on pure C_3S of a retarder that binds to calcium ions, [7]. The hydration of dicalcium silicate (C_2S), the other main component of oilwell cement, is very slow relative to that of C_3S, and we have not included it in our model.

In this paper, we will marry the model that we have developed for the hydration of pure C_3S in the presence of a retarder to our model for the inhibition of the growth of ettringite crystals, [4]. In addition, we will include the effect of the presence of calcium sulphate in the cement slurry. In the absence of calcium sulphate, once C_3A dissolves it undergoes a rapid 'flash set': a rapid reaction of the C_3S phase with water that sets hard so that the slurry cannot be pumped downhole. Calcium sulphate is added in order to provide sulphate ions in solution. These react preferentially with the dissolved aluminate ions, preventing a flash set and producing ettringite. Ettringite can exist either as an amorphous gel or as a crystal. The transition from the gel form, which presents a barrier to diffusion, to the crystalline form, which does not, is a key element of our model. Note that we are only considering the early stages of the retarded hydration process, as different reactions start to become important at later times.

Our principal aim in this paper is to show that, when incorporated into a model that includes the main, early-time chemical reactions and diffusive mass transport, the two effects of the retarder, namely complexing with calcium ions and poisoning of ettringite, can be incorporated into a rational model, and have a significant effect on the overall progress of hydration. We also want to investigate how these retarded reactions proceed, and whether the insights gained in [6] and [4] remain relevant in this more complex setting. This work should be viewed in the context of a variety of different models for cement hydration proposed by other authors, each of which is designed to address different aspects of the process. These models include early work on the hydration of C_3S, for example [8], more sophisticated studies of the development of microstructure in cement, for example [9] and [10], and recent attempts to build a comprehensive cement hydration simulator [11].

2. The mathematical model

We consider the dissolution of a spherical grain of cement. We assume that this grain consists of a homogeneous mixture of C_3S and C_3A, with a proportion δ of C_3A, and lies in the region $0 \leq r \leq r_1(t)$ in spherical polar coordinates. Chemical reaction occurs in the region $r_1(t) < r < r_2(t)$, and dissolution of the cement grain occurs at the surface $r = r_1(t)$. At $r = r_2(t)$, calcium and sulphate ions from the dissolution of calcium sulphate enter the reaction region, so that the solution remains saturated with sulphate ions there. This means that we have to solve a free-boundary problem to model the hydration process. Initially, this reaction region is occupied by water saturated with sulphate ions and with a uniform concentration of retarder. The subsequent evolution is assumed to be spherically symmetric, depending only upon r and time t. Since C_3S and C_3A dissolve at the surface of the grain, $r_1(t)$ decreases with time as the grain shrinks, releasing calcium, hydroxide, silicate and aluminate ions into solution. These ions are advected by a radial fluid velocity, which is included to take into account the effect of volume changes. They also diffuse and react chemically. The reactions that we include, which we will describe in detail in the next section are:

1. The precipitation of CSH, CH and ettringite.
2. The crystallisation of ettringite.

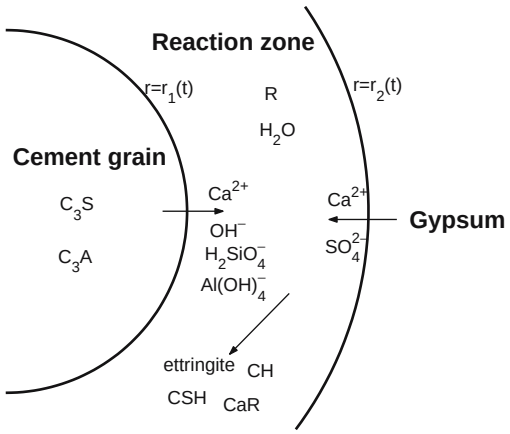

Figure 1. The positions of the two boundaries and the species involved in the reactions.

3. The action of the retarder to both inhibit the crystallisation of ettringite and bind with calcium ions.

The coordinate system and the various phases are illustrated in Figure 1.

A major difference between the model we describe here and that which we used in our earlier papers, [6] and [7], is that we work in terms of the mass fraction of each species, rather than its concentration. This allows us to include water, H, as another chemical species involved in the reaction, rather than just a background medium, relative to which the other species diffuse. We do this because the formation of ettringite is a thirsty process, consuming 26 moles of water for every mole of C_3A dissolved. In addition, we treat the solid and liquid phases separately, as we shall see in the next section. Although, in practice, cement hydration is a strongly exothermic reaction, we have not considered the effect of this here. Our focus is on the interplay of the various chemical reactions.

2.1. Mixture theory

We will use a mixture theory, based on that used in the context of multiphase flow (for example, [12]), where the solid and fluid phases are considered as interpenetrating media, and also based on the theory used in modelling combustion processes (for example, [13]). At each point, we define a liquid *volume* fraction, $\alpha(r,t)$, which measures the proportion of fluid there. Within the fluid phase, there are eight different species, with *mass* fractions $Y_i(r,t)$, for $i = 1, 2, \ldots, 8$, and

$$\sum_{i=1}^{8} Y_i = 1. \tag{1}$$

The species are labelled as

1. water, H,
2. sulphate ions, SO_4^{2-},
3. aluminate ions, $Al(OH)_4^-$,
4. retarder, R,
5. calcium ions, Ca^{2+},
6. hydroxide ions, OH^-,
7. silicate ions, $H_2SiO_4^{2-}$,
8. calcium/retarder complex, CaR.

We will assume that the density of the liquid phase, ρ_l, is constant. As we shall see, this is a key simplifying assumption, since it means that we do not need to solve a momentum equation. Unfortunately, this does mean that we should not expect the model to provide us with accurate data on how the total volume of the cement slurry changes with time. However, the fluid phase remains mainly water, and we would not expect its density to change enormously when the concentrations of the various ions change. Moreover, although the change in density will be important whilst the slurry is flowing and once it has been placed downhole, we are mainly concerned with the interplay between the chemical reactions.

In order to derive conservation equations for these eight species, we note that the total mass of each species between $r=a$ and $r=b$ is

$$M_i = 4\pi \int_a^b \rho_l \alpha(r,t) Y_i(r,t) r^2 \mathrm{d}r. \tag{2}$$

This changes with time due to both the flux of species i into and out of this volume, and to its consumption or production by chemical reaction or disassociation there. This means that

$$\frac{\mathrm{d}M_i}{\mathrm{d}t} = f_i(a,t)4\pi a^2 - f_i(b,t)4\pi b^2 + 4\pi \int_a^b Q_i r^2 \,\mathrm{d}r, \tag{3}$$

where $f_i(r,t)$ is the mass flux per unit area of species i, and Q_i its mass rate of production due to chemical reaction or disassociation. Since each species is transported by diffusion and advection alone, we write

$$f_i = \rho_l \alpha Y_i u - \mu\alpha \frac{\partial Y_i}{\partial r}, \tag{4}$$

where u is the radial fluid velocity and μ the diffusivity. In a multispecies model like this, if the diffusivities are not all taken to be equal, cross-species diffusion is needed in order to conserve mass. Although there is some variation in μ between the various ionic species, it is not large (see [14, Section 5]), so we make the simplifying assumption that the diffusivities of the ionic species are equal. After substituting (2) and (4) in (3) and integrating with respect to time, t, this gives us

$$\begin{aligned}\int_a^b \rho_l \alpha(r,t) Y_i(r,t) r^2 \mathrm{d}r\Big|_{t=t_2} - \int_a^b \rho_l \alpha(r,t) Y_i(r,t) r^2 \mathrm{d}r\Big|_{t=t_1} \\ = \int_{t_1}^{t_2} \left\{ \rho_l \alpha Y_i u - \mu\alpha \frac{\partial Y_i}{\partial r} \right\} a^2 \mathrm{d}t\Big|_{r=a} - \int_{t_1}^{t_2} \left\{ \rho_l \alpha Y_i u - \mu\alpha \frac{\partial Y_i}{\partial r} \right\} b^2 \mathrm{d}t\Big|_{r=b} + \int_{t_1}^{t_2} \int_a^b Q_i r^2 \mathrm{d}r\mathrm{d}t.\end{aligned} \tag{5}$$

It is straightforward to convert this integral conservation law into an advection-reaction-diffusion partial differential equation by writing $a=r$, $b=r+\delta r$, $t_1=t$ and $t_2=t+\delta t$, and taking the limits $\delta r \to 0$ and $\delta t \to 0$. This gives us

$$\rho_l \left\{ \frac{\partial}{\partial t}(\alpha Y_i) + \frac{1}{r^2}\frac{\partial}{\partial r}\left(r^2 \alpha Y_i u \right) \right\} = \frac{1}{r^2}\frac{\partial}{\partial r}\left(r^2 \mu\alpha \frac{\partial Y_i}{\partial r} \right) + Q_i, \tag{6}$$

but (5) is actually the most convenient form to use when constructing a numerical solution scheme using the finite-volume method (see, for example, [15 Chapter 1]).

In the solid phase, which has volume fraction $1-\alpha(r,t)$, there are five species with mass fractions $\bar{Y}_j$ for $j=1,2,3,4,5$, and

$$\sum_{j=1}^{5} \bar{Y}_j = 1. \tag{7}$$

The species are labelled as
1. ettringite gel,
2. crystalline ettringite,
3. ettringite.R = poisoned ettringite,
4. CSH gel,
5. calcium hydroxide, CH.

In our simulations we have modelled the diffusivity of the ions as

$$\mu = \mu_1 + (\mu_0 - \mu_1) \exp\left\{-k_d(1-\alpha)\bar{Y}_1\right\}, \tag{8}$$

where $\mu_0 \gg \mu_1$ and k_d are constants. In this way, the diffusivity decreases from μ_0 to μ_1 as the total amount of ettringite gel, $(1-\alpha)\bar{Y}_1$, at each point increases.

As for the liquid phase, we assume that the density of the solid phase, ρ_s, is constant. There is no advection or diffusion of these solid species, so, by analogy with (5) and (6), we have

$$\int_a^b \rho_s\,(1-\alpha(r,t))\,\bar{Y}_j(r,t)r^2\mathrm{d}r\bigg|_{t=t_2} - \int_a^b \rho_s\,(1-\alpha(r,t))\,\bar{Y}_j(r,t)r^2\mathrm{d}r\bigg|_{t=t_1} = \int_{t_1}^{t_2}\int_a^b \bar{Q}_j r^2 \mathrm{d}r\mathrm{d}t, \tag{9}$$

or equivalently,

$$\rho_s \frac{\partial}{\partial t}\left\{(1-\alpha)\,\bar{Y}_j\right\} = \bar{Q}_j. \tag{10}$$

We can obtain an equation that describes the rate of expansion of the mixture by adding (10) for $j = 1$ to 5, and using (7), which gives us

$$\frac{\partial \alpha}{\partial t} = -\frac{Q_s}{\rho_s}, \tag{11}$$

where

$$Q_s = \sum_{j=1}^{i=5} \bar{Q}_j \tag{12}$$

is the rate at which liquid mass is converted to solid mass. Similarly, if we add (6) for $i = 1$ to 8 and use (1) and (12), we find that

$$\frac{1}{r^2}\frac{\partial}{\partial r}\left(r^2 \alpha u\right) = \left(\frac{1}{\rho_s} - \frac{1}{\rho_l}\right) Q_s, \tag{13}$$

which determines how the radial velocity, u, changes as liquid mass is converted to solid mass. Note that we must have

$$Q_s = \sum_{i=1}^{8} Q_i, \tag{14}$$

since the rate at which liquid mass is consumed is equal to the rate at which solid mass is created. We can verify that (12) and (14) are consistent once we have postulated reaction rate laws for the individual reaction steps.

2.2. Chemical kinetics

In the bulk, seven chemical reactions take place. In the following rate laws, k_i for $i = 1, 2, \ldots, 7$ are reaction rate constants. We use a variety of different types of reaction-rate laws, depending upon the type of reaction step that we are trying to model. As we shall see later, by choosing the rate constants appropriately, we can generate solutions that are in qualitative agreement with experimental observations. Note that we shall assume that these reactions are not reversible to keep the model as simple as possible, consistent with wanting to investigate the interaction of the various important chemical processes.

1. $H_2SiO_4^{2-} + \frac{3}{2}Ca^{2+} + OH^- + H_2O \rightarrow CSH$, rate $q_1 = k_1 Y_1 (Y_5 Y_6 Y_7)^{2/3} \alpha^3$. Note that, in contrast to our earlier models, we have used a reaction-rate law with a power-law dependence on the mass fractions. This is simpler to implement on the type of moving grid that we will use later in our numerical solution. It is not reasonable to use the law of mass action for such complex, multispecies reactions.
2. $2Al(OH)_4^- + 6Ca^{2+} + 4OH^- + 3SO_4^{2-} + 26H_2O \rightarrow (1-\epsilon)\,ett^g + \epsilon\, ett^c$, rate $q_2 = k_2 Y_1 (Y_2 Y_3 Y_5 Y_6)^{1/2} \alpha^3$. Note that we choose the power-law dependences of q_1 and q_2 to be quadratic in the ionic species and linear in Y_1, the mass fraction of water. We chose this quadratic dependence so that the reaction rate was of the same overall order in terms of the ions as the ettringite reaction steps that we describe below. In addition, ettringite is produced mainly as gel, ett^g, but with a small constant proportion, $\epsilon \ll 1$, of crystalline ettringite, ett^c.
3. $ett^g + ett^c \rightarrow 2ett^c$, rate $q_3 = k_3(1-\alpha)^2 \bar{Y}_1 \bar{Y}_2$. This is the autocatalytic step that produces more crystalline ettringite from the small fraction seeded by the previous reaction. The use of the law of mass action for this step is discussed in [4].
4. $ett^c + R \rightarrow ett^p$, rate $q_4 = k_4 \alpha (1-\alpha) \bar{Y}_2 Y_4$. This is the step through which the retarder inhibits the production of crystalline ettringite by binding with it to produce a poisoned form, ett^p. In [4] it was shown that a quadratic autocatalytic model for the ettringite gel to crystalline transition along with a quadratic inhibition step leads to clock reaction-like behaviour, with a long induction phase followed by a rapid transition phase. We use the law of mass action for each of the two- and three-component steps 4, 5 and 7.
5. $Ca + R \rightarrow CaR$, rate $q_5 = k_5 \alpha^2 Y_4 Y_5$. The retarder forms a complex, CaR, with calcium ions in this step. We assume that this complex cannot inhibit the growth of crystalline ettringite.
6. $Ca^{2+} + 2OH^- \rightarrow CH$, rate $q_6 = k_6 \alpha^3 \left(Y_5 Y_6^2 - Y_{56sat}^3\right) \mathcal{H}\left(Y_5 Y_6^2 - Y_{56sat}^3\right)$. Calcium hydroxide, CH, is formed through a precipitation reaction once the solubility product, $Y_5 Y_6^2$, exceeds the saturated value, Y_{56sat}^3. Note that $\mathcal{H}$ is the Heaviside step function.
7. $Ca^{2+} + 2OH^- + CH \rightarrow 2CH$, rate $q_7 = k_7 \alpha^2 (1-\alpha) Y_5 Y_6 \bar{Y}_5$. This is an autocatalytic step, which will dominate the production of CH once CH itself is formed in the previous step.

From these rate laws we can deduce Q_i and $\bar{Q}_j$. In particular, the rate at which liquid mass is converted to solid mass is

$$Q_s = \bar{m}_4 q_1 + \{(1-\epsilon)\,\bar{m}_1 + \epsilon \bar{m}_2\}\, q_2 + m_4 q_4 + \bar{m}_5 (q_6 + q_7), \tag{15}$$

where m_i are the molar masses of the ionic species, and $\bar{m}_j$ the molar masses of the solid species. As we would expect, the conversion of ions to ettringite and CSH gels and to calcium hydroxide, along with the incorporation of the retarder into the structure of poisoned ettringite, are the only processes that contribute to Q_s. To summarize, we have used the law of mass action for the ionic reaction rates, in line with the work discussed in [4], [16] and [7],

power-law reaction rates compatible with these and solubility product type reaction rates for the precipitation reactions, as discussed in [6].

At the boundary $r = r_1(t)$, we assume that the dissolution of both C_3S and C_3A,

$$C_3S + 3H_2O \rightarrow 3Ca^{2+} + 4OH^- + H_2SiO_4^{2-}, \tag{16}$$

$$C_3A + 6H_2O \rightarrow 3Ca^{2+} + 4OH^- + 2Al(OH)_4^-, \tag{17}$$

proceeds at the same rate, $q_0 = k_0 \alpha Y_1 \exp\left\{-K_0 (Y_3 + Y_7) Y_5 Y_6 / Y_{\text{sat}}^3\right\}$, evaluated at $r = r_1(t)$, with k_0 and K_0 constants. This means that the rate of dissolution decreases as $\{(Y_3 + Y_7) Y_5 Y_6\}^{1/3}$ approaches Y_{sat} and the solution becomes saturated. Note that this is an effect that we had to build into our earlier model, [6], in a somewhat artificial manner. Of course, within the context of our model of the cement grain as a continuous sphere of uniform composition, it is not possible to allow the two constituents to dissolve at unequal rates, so this should be treated as a simplifying assumption.

The boundary, $r = r_1(t)$, of the grain shrinks as this dissolution occurs, with

$$\frac{dr_1}{dt} = V_1 = -\frac{\delta M_1 + (1-\delta) M_2}{\rho_c} q_0, \tag{18}$$

where ρ_c is the density of the grain, δ is the proportion of C_3A in the grain and

$$M_1 = 3m_5 + 4m_6 + 2m_3 - 6m_1, \quad M_2 = 3m_5 + 4m_6 + m_7 - 3m_1$$

are the molar masses of C_3A and C_3S. The boundary conditions at $r = r_1(t)$ are that there is no flux of retarder, sulphate ions or retarder/calcium complex, and that the fluxes of calcium, hydroxide, silicate and aluminate ions, and water, are consistent with (16) and (17). This means that

$$\begin{aligned}
&\mu\alpha \frac{\partial Y_1}{\partial r} = \rho_l \alpha (u - V_1) Y_1 + 3(1+\delta) m_1 q_0, \quad \mu\alpha \frac{\partial Y_2}{\partial r} = \rho_l \alpha (u - V_1) Y_2, \\
&\mu\alpha \frac{\partial Y_3}{\partial r} = \rho_l \alpha (u - V_1) Y_3 - 2\delta m_3 q_0, \quad \mu\alpha \frac{\partial Y_4}{\partial r} = \rho_l \alpha (u - V_1) Y_4, \\
&\mu\alpha \frac{\partial Y_5}{\partial r} = \rho_l \alpha (u - V_1) Y_5 - 3m_5 q_0, \quad \mu\alpha \frac{\partial Y_6}{\partial r} = \rho_l \alpha (u - V_1) Y_6 - 4m_6 q_0, \\
&\mu\alpha \frac{\partial Y_7}{\partial r} = \rho_l \alpha (u - V_1) Y_7 - (1-\delta) m_7 q_0, \quad \mu\alpha \frac{\partial Y_8}{\partial r} = \rho_l \alpha (u - V_1) Y_8
\end{aligned} \tag{19}$$

at $r = r_1(t)$. If we add these boundary conditions and make use of (1), (7) and (18), we find that

$$u(r_1, t) = \left(\frac{1}{\rho_l \alpha(r_1, t)} - \frac{1}{\rho_c} \right) \{\delta M_1 + (1-\delta) M_2\} q_0. \tag{20}$$

In order to determine the boundary conditions at $r = r_2(t)$, we note that calcium sulphate dissolves through the reaction

$$CaSO_4 \rightarrow Ca^{2+} + SO_4^{2-}.$$

Although this reaction is reversible, and could lead to the precipitation of gypsum, we have excluded this possibility, since gypsum is added specifically to provide sulphate ions and prevent flash set, as discussed earlier. We assume that there is a flux of calcium and sulphate ions through $r = r_2(t)$ in equal proportions, such that the mass fraction of sulphate ions, $Y_2(r_2, t)$, remains at its saturated value, $Y_{2\text{sat}}$. We therefore require that

$$\frac{dr_2}{dt} = V_2, \tag{21}$$

$$Y_2 = Y_{2\mathrm{sat}}, \tag{22}$$

and

$$\mu\alpha\frac{\partial Y_1}{\partial r} = \rho_l\alpha\,(u - V_2)\,Y_1, \quad \mu\alpha\frac{\partial Y_2}{\partial r} = \rho_l\alpha\,(u - V_2)\,Y_2 + m_2 q_G,$$

$$\mu\alpha\frac{\partial Y_3}{\partial r} = \rho_l\alpha\,(u - V_2)\,Y_3, \quad \mu\alpha\frac{\partial Y_4}{\partial r} = \rho_l\alpha\,(u - V_2)\,Y_4,$$

$$\mu\alpha\frac{\partial Y_5}{\partial r} = \rho_l\alpha\,(u - V_2)\,Y_5 + m_5 q_G, \quad \mu\alpha\frac{\partial Y_6}{\partial r} = \rho_l\alpha\,(u - V_2)\,Y_6,$$

$$\mu\alpha\frac{\partial Y_7}{\partial r} = \rho_l\alpha\,(u - V_2)\,Y_7, \quad \mu\alpha\frac{\partial Y_8}{\partial r} = \rho_l\alpha\,(u - V_2)\,Y_8$$

at $r = r_2(t)$, where V_2 is the velocity of the outer boundary and q_G is the flux of ions due to the dissolution of calcium sulphate, both of which are to be determined. The most useful way of writing these is to eliminate q_G to give

$$\mu\alpha\frac{\partial Y_1}{\partial r} = \rho_l\alpha\,(u - V_2)\,Y_1, \quad \mu\alpha\frac{\partial Y_3}{\partial r} = \rho_l\alpha\,(u - V_2)\,Y_3,$$

$$\mu\alpha\frac{\partial}{\partial r}\,(m_2 Y_5 - m_5 Y_2) = \rho_l\alpha\,(u - V_2)\,(m_2 Y_5 - m_5 Y_2)\,, \tag{23}$$

$$\mu\alpha\frac{\partial Y_4}{\partial r} = \rho_l\alpha\,(u - V_2)\,Y_4, \quad \mu\alpha\frac{\partial Y_6}{\partial r} = \rho_l\alpha\,(u - V_2)\,Y_6,$$

$$\mu\alpha\frac{\partial Y_7}{\partial r} = \rho_l\alpha\,(u - V_2)\,Y_7, \quad \mu\alpha\frac{\partial Y_8}{\partial r} = \rho_l\alpha\,(u - V_2)\,Y_8$$

at $r = r_2$. There are 10 unknowns at $r = r_2$, namely r_2, V_2 and Y_i for $i = 1, 2, \ldots, 8$, and 10 equations, seven in (23), along with (1), (21) and (22).

Finally, we note that appropriate initial conditions are that

$$r_1 = r_{10}, \quad r_2 = r_{20}, \quad Y_3 = Y_5 = Y_6 = Y_7 = Y_8 = 0,$$
$$Y_2 = Y_{2sat}, \quad Y_4 = Y_{40}, \quad Y_1 = 1 - Y_{2sat} - Y_{40}, \quad \alpha = 1, \tag{24}$$

when $t = 0$. Note that we do not need to specify $\bar{Y}_j$, since $\alpha = 1$ (everything is in the liquid phase initially).

The mass fractions and the liquid volume fraction are already dimensionless, so there is not much work to do to make our system of equations dimensionless. We use the initial radius of the grain, r_{10} as our lengthscale, and make a timescale using the rate of dissolution of the grain and the molar mass and density of ettringite, $\bar{m}_1 k_0/\rho_s$. This leads to a velocity scale $\rho_s r_{10}/\bar{m}_1 k_0$ and a diffusion scale $\bar{m}_1 k_0 r_{10}^2$. The dimensionless constants that remain in the system are then ratios of reaction rate constants, molar masses and diffusion rates. This is equivalent to setting $r_{10} = 1$, $k_0 = 1$, $\mu_0 = 1$ and $\bar{m}_1 = \bar{m}_2 = 1$.

3. Numerical solution method

The simplest numerical solution method would be to discretize the region $r_1(t) \le r \le r_2(t)$ with a uniform grid of $N + 1$ points, $r = r_{(I)} = r_1 + (I - 1)\Delta r$ for $I = 1, 2, \ldots N + 1$, with $\Delta r = (r_2 - r_1)/N$. However, we need to take into account the motion of the inner and outer boundaries, $r = r_1(t)$ and $r = r_2(t)$. We therefore allow the first and last grid points, $r_{(1)}$ and

$r_{(N+1)}$, to move with the solid and fluid, respectively, whilst keeping the other grid points fixed. Whenever either of these boundary points moves far enough that it is more than $1{\cdot}01\Delta r$ away from its nearest neighbour, we regrid onto a new uniform grid, with a new value of Δr, and linearly interpolate all of the dependent variables onto the new grid.

We use a finite-volume method, with the liquid-volume fraction, α, and the species mass fractions, Y_i and $\bar{Y}_j$, calculated at the midpoints of each cell. In fact, as we can see from the form of the Equations (9) and the forms of the reaction rates, it is more convenient to work with $Z_j = (1-\alpha)\,\bar{Y}_j$, which are zero initially. In addition, it is more sensible to discretize the radial fluid velocity, u, at the boundaries of the cell, so that $u = u_I$ at $r = r_{(I)}$.

We will now sketch the solution method that we have used. The method is explicit in time and, for (13), explicit in space. At each time step we move the grid points at r_1 and r_2 using $r_{1,2}(t+\Delta t) = r_{1,2}(t) + \Delta t\, V_{1,2}$, where Δt is the time step, and solve on cells bounded by these two points and the original cell boundaries. At each time step, we calculate the reaction rates and diffusion coefficient using the known species fractions.

The method is based on discretizing the integral conservation laws (5) and (9). For example, on the part of the domain with cells of equal length, (5) gives

$$\frac{\rho_l\left(\alpha_I^{t+\Delta t}Y_I^{t+\Delta t} - \alpha_I^t Y_I^t\right) r_{I+\frac{1}{2}}^2}{\Delta t} = \frac{r_I^2 f_{I-\frac{1}{2}}^t - r_{I+1}^2 f_{I+\frac{1}{2}}^t}{\Delta r} + r_I^2 Q_I^t, \tag{25}$$

where the subscripts refer to the cell and the superscripts to time and

$$f_{I+\frac{1}{2}} = \alpha_{I+\frac{1}{2}}\left(\rho_l u_{I+1} Y_{I+\frac{1}{2}} - \mu_{I+\frac{1}{2}}\frac{Y_{I+1}-Y_I}{\Delta r}\right), \tag{26}$$

$$Y_{I+\frac{1}{2}} = \frac{1}{2}\left(Y_I + Y_{I+1}\right), \quad \alpha_{I+\frac{1}{2}} = \frac{1}{2}\left(\alpha_I + \alpha_{I+1}\right), \quad r_{I+\frac{1}{2}} = \frac{1}{2}\left(r_I + r_{I+1}\right). \tag{27}$$

At the end cells, $I = 1$ and $I = N+1$, whose boundaries move, we need to be a little more careful, since the cell sizes change with time and we need to use the fluxes prescribed by (19) and (23). For example, at $r = r_1$, taking into account the geometry of the old and new cells, we find that

$$\begin{aligned}&\Delta r_1 \rho \alpha_1^{t+\Delta t} Y_1^{t+\Delta t}\left(r_1^{t+\Delta t}\right)^2 - \Delta r_0 \rho \alpha_1^t Y_1^t \left(r_1^t\right)^2 \\ &\quad = \Delta t\left(f_{\frac{3}{2}}^t\left(r_{\frac{3}{2}}^t\right)^2 - f_1^t\left(r_1^t\right)^2\right) + \frac{1}{2}\Delta t\left(\Delta r_0 + \Delta r_1\right)\left(r_1^t\right)^2 Q_1^t,\end{aligned} \tag{28}$$

where $\Delta r_0 = r_{(2)}^t - r_{(1)}^t$ and $\Delta r_1 = r_{(2)}^{t+\Delta t} - r_{(1)}^{t+\Delta t}$. The flux f_1 at $r = r_1$ is then given by the boundary conditions at $r = r_1$, (19), and similarly at $r = r_2$.

We begin by solving for the liquid fraction, α, on the new set of cells, then solve for u by discretizing (13) explicitly in space, stepping in the positive r-direction from the known value at $r = r_1$ given by (20). We then solve for Y_i and Z_j. In this way, we can ensure that we conserve mass to machine accuracy.

Determining the new values at $r = r_2$ is more troublesome, since we do not have an explicit expression for V_2. We use an iterative method, taking an initial guess of V_2, solving at $r = r_2(t+\Delta t)$, and determining the value of Y_2 there. We then modify V_2 until $Y_2 = Y_{2\mathrm{sat}}$ using the secant method. The final step is to check whether either of the end points has moved far enough that we need to define a new, uniform grid on $r_1(t+\Delta t) \le r \le r_2(t+\Delta t)$. If so, we linearly interpolate the variables onto this new grid. Although this does not conserve mass to machine accuracy, the loss of mass is small, as we shall see later. Finally, note that we choose

an appropriate time step at each stage by considering the usual stability constraint on this explicit discretization, and also from the size of the reaction rate terms. In addition, if any of the quantities changes by more than a small threshold value at any time step, we repeat with the time step halved.

4. Numerical results

We have yet to compare our model quantitatively with experimental data; indeed, this is a very difficult task given the complexity of the system and the difficulties of measuring the quantities that we model, so the following results are simply intended to give some idea of the type of behaviour that the model predicts. The results are qualitatively in agreement with what is observed experimentally, [3, Chapter 11].

Working in terms of the dimensionless variables that we defined above, we used $r_{20} = 2{\cdot}5$, which corresponds to a water/cement ratio by mass of about 5 and $\delta = 0{\cdot}25$; a grain that is 25% C_3A. We calculated the molar masses of the various chemicals from those of their constituents, and used $\epsilon = 0{\cdot}001$, $k_1 = 3 \times 10^4$, $k_2 = 3 \times 10^3$, $k_3 = 10^2$, $k_4 = 10^4$, $k_5 = 3 \times 10^3$, $k_6 = 10^3$, $k_7 = 10^6$, $K_0 = 2$, $\rho_l/\rho_s = 0{\cdot}65$, $\rho_c/\rho_s = 2$, $k_d = 50$, $\mu_0 = 10^{-1}$, $\mu_1 = 10^{-2}$, $Y_{2\mathrm{sat}} = 0{\cdot}02$, $Y_{\mathrm{sat}} = 0{\cdot}005$ and $Y_{56\mathrm{sat}} = 0{\cdot}004$. Some of these dimensionless reaction-rate constants are rather large, but only because the mass fractions of some of the ions are rather small. We could have scaled the various mass fractions, which would have led to smaller dimensionless reaction rates, but there is little value in this, since we are proceeding numerically.

We will describe four simulations, with the initial mass fraction of retarder being successively $Y_{40} = 0$, $0{\cdot}025$, $0{\cdot}05$ and $0{\cdot}075$. The simulations discussed below used 200 cells and proceeded until $t = 1000$. However, we also ran some shorter simulations with more cells to check that the solution we obtained had converged at this level of resolution. Animations of the evolution of the solid and liquid fractions, which give more of a feel for how the solution develops, can be found at http://www.maths.nott.ac.uk/personal/pmzjb1/cementanimations.htm. Figures 2 to 11 illustrate various aspects of the solutions.

In the absence of any retarder, most of the ettringite gel that forms is immediately transformed to crystalline ettringite, as shown in Figure 2, and the solid fraction rapidly increases, as shown in Figure 3. The calcium and hydroxide ion concentrations build up in solution, as shown in Figures 4 and 5. When $t \approx 10$, calcium hydroxide starts to precipitate at the surface

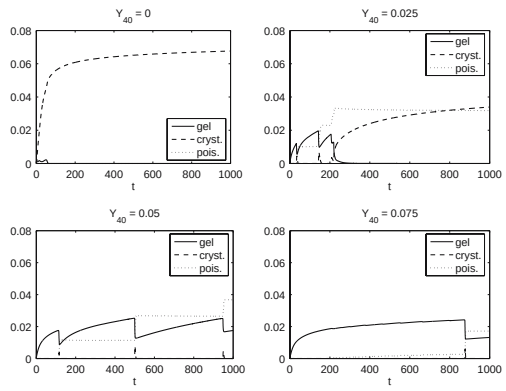

Figure 2. The dimensionless total amounts of the solid constituents as functions of time.

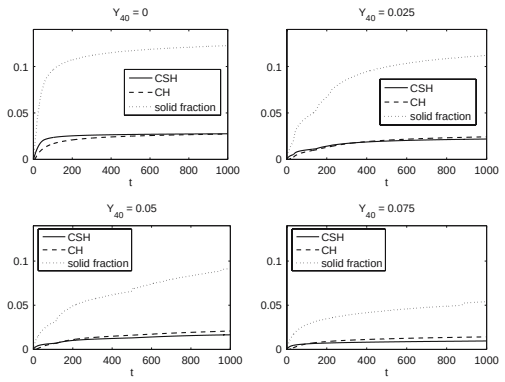

Figure 3. The dimensionless total amounts of the solid constituents as functions of time.

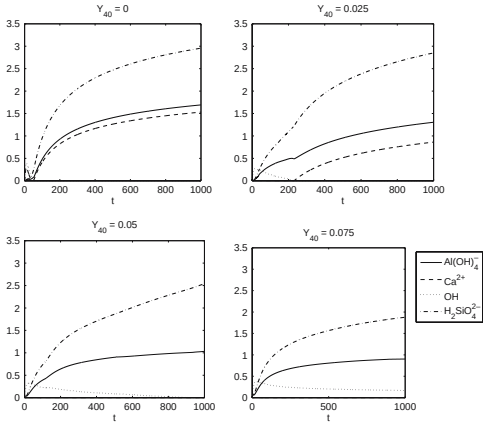

Figure 4. The dimensionless total amounts of the ionic constituents as functions of time.

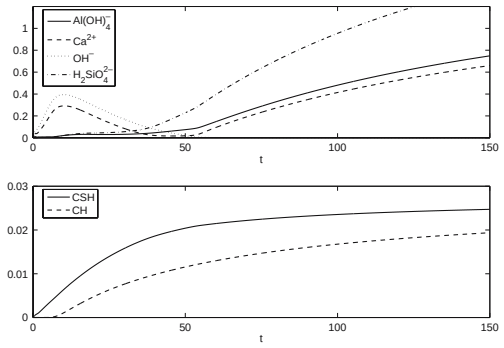

Figure 5. The solution for $t \leq 150$ when no retarder is present ($Y_{40} = 0$).

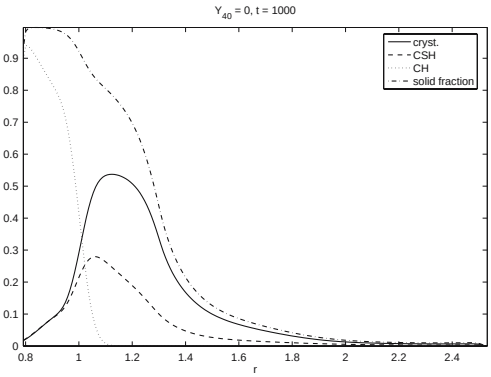

Figure 6. The distribution of the solid phases when $t = 1000$, with no retarder.

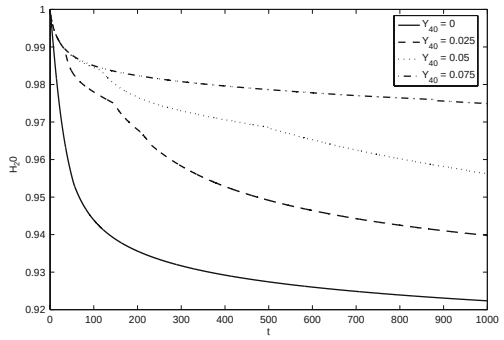

Figure 7. The total amounts of water as a function of time, scaled so that the initial amount is 1.

of the grain, and the concentrations of hydroxide and calcium ions start to decrease, whilst silicate and aluminate ions build up in solution. When $t \approx 60$, all of the hydroxide ions in solution away from the surface of the grain have been consumed, and these only exist in the neighbourhood of the grain. This allows the concentration of calcium ions to increase again. As the surface of the grain recedes, the layer of solids, a mixture of CSH gel, ettringite and CH, builds up, as shown in Figure 6. At some later time, dependent upon the interactions of the grains when the slurry is in motion, it will no longer be possible to pump the cement. Figure 7 shows that 8% of the initial water has been consumed when $t = 1000$. Figure 8 shows the positions of the boundaries of the domain. When $t = 1000$, $r_1 \approx 0{\cdot}78$, which means that more than half of the volume of the grain has been consumed in the reaction by this time. Figure 9 shows the fluid velocity, u, when $t = 50$. The maximum close to the surface of the grain is due to the large solid fraction there, which leads to an increased fluid velocity in order to maintain continuity of flux, αu. The velocity profile is qualitatively similar throughout the hydration process.

The most obvious effect of the retarder is that it forms a complex with calcium ions, so that there is very little calcium in solution away from the surface of the grain (see Figure 4).

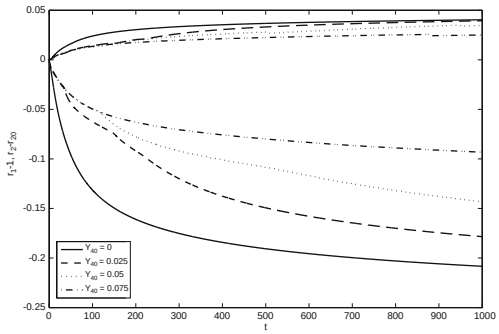

Figure 8. The changes in the positions of the inner and outer boundaries as functions of time.

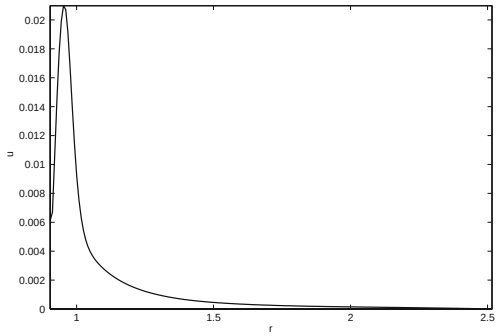

Figure 9. The fluid velocity, u, for the unretarded reaction when $t = 50$.

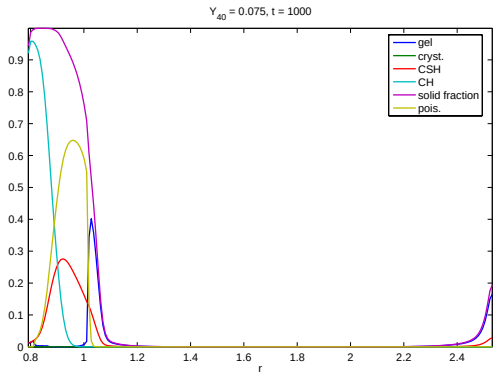

Figure 10. The distribution of the solid phases when $t = 1000$, with $\bar{Y}_{40} = 0{\cdot}075$.

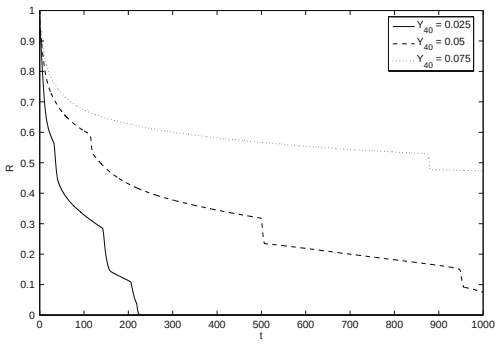

Figure 11. The total amounts of retarder as a function of time, scaled so that the initial amount is 1.

This leads to significantly higher concentrations of hydroxide in solution than in the unretarded case. In addition, although some of the ettringite gel is transformed to crystalline ettringite, and is then poisoned by the retarder, there is a significant concentration of ettringite gel a small distance from the surface of the grain, which is not transformed to crystalline ettringite because of the action of the retarder. As time passes, at discrete intervals, successive layers of this gel are transformed to crystalline ettringite. This can be seen clearly in Figure 2, where, although the total amounts of the various forms of ettringite appear to change discontinuously, these changes are in fact smooth when examined on a finer time scale. These rapid changes arise because of the interaction between the autocatalytic production of ettringite crystals from ettringite gel in the presence of the inhibitor, as described in [4] and [16]. The transformation occurs in successive layers as time progresses. This is illustrated in Figure 10, which shows the distribution of the solid phases when $t = 1000$. There is a layer of poisoned ettringite surrounded by a layer of ettringite gel, which has yet to be transformed to its crystalline form. The presence of significant amounts of ettringite gel decreases the diffusion coefficient, and traps a higher concentration of ions close to the surface of the grain. One consequence of this is that the grain dissolves more slowly, as shown in Figure 8. This means that the total amount of solid formed is larger in the unretarded case, which means that the thickening time is shorter, as we should expect, as shown in Figure 2. Once the retarder is consumed (see Figure 11), the reaction proceeds along the same lines as the unretarded case.

Note also that, as shown in Figure 10, when there is sufficient retarder present that a significant concentration of hydroxide ions persists in solution, some ettringite may form at the outer boundary of the domain.

5. Conclusions and future work

We have been able to construct a multiphase, multicomponent model for the hydration of oilwell cement in the presence of a retarder. Furthermore, we have shown that the two effects of a retarder, namely complexing with calcium and poisoning of ettringite are not mutually exclusive, and can both act to retard the hydration process. The most pressing need is to quantitatively compare our results with experimental data, and we are currently pursuing this. It would also be of interest to investigate the spatial structure of the gel to crystalline transition that occurs at discrete time intervals in the model. Some related work is discussed in [17].

Once we have estimated the various parameters in the model, mainly the unknown reaction rate constants, we can consider extensions to the current model. Possible avenues to explore include:

- Extension of the model to a periodic array of grains, which requires the solution of the fully three-dimensional version of the model equations instead of the simpler, spherically symmetric problem that we have considered so far.
- The inclusion of other chemical reactions, which may be important for cements used in industries other than the oil industry.
- Modelling the volume change of the cement. This would require a completely different numerical scheme, since a momentum equation along with density as a function of pressure and composition would be required. This would also be the appropriate point at which to bring the effect of temperature changes due to exothermicity into the model.

References

1. E. Nelson (ed.), *Well Cementing*. Houston: Schlumberger Educational Services (1990) 496 pp.
2. V.S. Ramachandran, M.S. Lowery, T.Wise and G.M. Polomark, The role of phosphonates in the hydration of Portland cement. *Mater. Struct.* 26 (1993) 425–432.
3. H.F.W. Taylor, *Cement Chemistry*. London: Academic Press (1997) 475 pp.
4. J. Billingham and P.V. Coveney, Simple chemical clock reactions: application to cement hydration. *J. Chem. Soc. Faraday Trans.* 89 (1993) 3021–3028.
5. P.V. Coveney and W. Humphries, Modelling of the mechanism of action of phosphonate retarders on hydrating cements. *J. Chem. Soc. Faraday Trans.* 92 (1996) 831–841.
6. S.J. Preece, J. Billingham and A.C. King, On the initial stages of cement hydration. *J. Engng. Math.* 40 (2001) 43–58.
7. A. Salhan, J. Billingham and A.C. King, The effect of a retarder on the early stages of the hydration of tricalcium silicate. *J. Engng. Math.* 45 (2003) 367–377.
8. J.M. Pommersheim and J.R. Clifton, Mathematical modelling of tricalcium silicate hydration. *Cem. Conc. Res.* 9 (1979) 765–770.
9. P. Navi and C. Pignat, Simulation of cement hydration and the connectivity of the capillary pore space. *Adn. Cem. Bas. Mat.* 4 (1996) 58–67.
10. G. Ye, P. Lura, K. van Breugel and A.L.A. Fraaij, Study on the development of the microstructure in cement-based materials by means of numerical simulation and ultrasonic pulse velocity measurement. *Cem. Conc. Comp.* 26 (2004) 491–497.
11. D.P. Bentz, Three-dimensional computer simulation of Portland cement hydration and microstructure development. *J. Am. Ceram. Soc.* 80 (2001), 3–21.
12. D.A. Drew and S.L. Passman, *Theory of Multicomponent Fluids.* New York: Springer Verlag (1999) 308 pp.

13. J.D. Buckmaster and G.S.S. Ludford, *Theory of Laminar Flames.* Cambridge: Cambridge University Press (1982) 280 pp.
14. D.R. Lide (ed.), *CRC Handbook of Chemistry and Physics (85th ed.)*. Baton Rouge: CRC Press (2004) 2712 pp.
15. R.J. LeVeque, *Finite Volume Methods for Hyperbolic Problems*. Cambridge: Cambridge University Press, (2002) 558 pp.
16. J. Billingham and D.J. Needham, Mathematical modelling of chemical clock reactions. II. A class of auto-catalytic clock reaction schemes. *J. Engng. Math.* 27 (1993) 113–145.
17. S.J. Preece, J. Billingham and A.C. King, The evolution of travelling waves from chemical-clock reactions. *J. Engng. Math.* 39 (2001) 367–385.